Clays and Clay Minerals, Vol. 49, No. 2, 156–167, 2001.

ILLITE "CRYSTALLINITY" REVISITED

M. JABOYEDOFF,[1,2] F. BUSSY,[1] B. KÜBLER,[2]† AND PH. THELIN[1]

[1]Institut de Minéralogie et Pétrographie, Université de Lausanne, BFSH2, 1015 Lausanne, Switzerland
[2]Institut de Géologie, Université de Neuchâtel, Rue Emile-Argand, 11, 2007 Neuchâtel, Switzerland

Abstract—The Kübler Index (KI) is defined as the full width at half-maximum height (FWHM) of the 10-Å X-ray diffraction peak of illite-smectite interstratified (I–S) clay minerals. The only parameters controlling the Kübler Index are assumed to be the mean number of layers (N) in the coherent scattering domains (CSD), the variance of the distribution of the number of layers of the CSD, the mean percentage of smectite layers in I–S (%S), and the probability of layer stacking (Reichweite).

The Kübler-Index measurements on air-dried (KIAD) and ethylene-glycolated (KIEG) samples were compared to N and %S using the NEWMOD computer program to simulate X-ray diffraction patterns. Charts of KIAD *versus* KIEG corrected for instrumental broadening were made and isolines were mapped for constant N and %S. Isolines allow a direct and rapid determination of N and %S from KI measurements.

The method allows quantification of the metamorphic anchizone limits by considering mean thickness of fundamental particles in MacEwan crystallites. The transition from diagenesis to the anchizone and from the anchizone to the epizone of low-grade metamorphism corresponds to thicknesses of 20- and 70-layer fundamental particles, respectively.

Key Words—Anchizone, Coherent Diffracting Domain Thickness, Expandable Layer, Fundamental Particles, Illite "Crystallinity", Illite-Smectite Interstratification.

INTRODUCTION

The Kübler Index (KI) is the full width at half-maximum height (FWHM) of the illite 10-Å X-ray diffraction (XRD) peak, measured on the <2-μm size fraction of an air-dried clay specimen using CuKα radiation (Kübler, 1964, 1967, 1968, 1984). KI is expressed as Δ°2θ CuKα. The KI measurement is made here by interpolating the background under the peak by connecting the background on both sides of the peak. Measurements of illite "crystallinity" (IC) are widely used as an indicator of incipient metamorphism, and values decrease with increasing metamorphic grade. This trend has been correlated with changing metamorphic mineral assemblages and also with indicators of organic maturity (Kübler, 1967, 1984; Jaboyedoff and Thélin, 1996; Merriman and Frey, 1999). The index introduced by Kübler (1964, 1967, 1968) quickly became popular and is widely used because of its simplicity and reproducibility. Other XRD-based methods relying on migrating peaks of interstratified illite-smectite (I–S) (*e.g.,* Środoń and Eberl, 1984; Watanabe, 1988) were inaccurate for highly illitic I–S. The KI is also an improvement of the Weaver index, the ratio of peak intensities measured at 10.0 and 10.5 Å on air-dried samples (Weaver, 1960), which was found to be less accurate experimentally (Kübler, 1967).

KI is used to characterize the transition from diagenesis to low-grade metamorphism, *i.e.,* from late diagenesis through the anchizone to the epizone, which is equivalent to low greenschist facies metamorphism. The limits of the anchizone, the zone of incipient or very low-grade metamorphism, are defined on the KI scale at 0.42°Δ2θ CuKα for the diagenesis/anchizone boundary, and at 0.25°Δ2θ CuKα for the anchizone/epizone boundary. These limits were originally defined by Kübler (1967), but measured values vary depending on the type of diffractometer used.

Although illite "crystallinity" measurements are still widely used, many investigators also use peak decomposition methods in the 10-Å region (*e.g.,* Lanson, 1990, 1997; Wang *et al.,* 1995). The peak decomposition method involves matching an observed peak shape with a calculated shape based on various mathematical functions (*e.g.,* Gaussian, Lorentzian, Pearson VII, *etc.*) for the individual calculated peak components (Howard and Preston, 1989; Lanson, 1990, 1997; Wang *et al.,* 1995). Refinement by least-squares is performed after subtraction of the background and removal of the $CuK\alpha_2$ radiation contribution from the observed diffraction pattern. KI measurements may be made on the decomposed peaks (Lanson and Velde, 1992), but new values for metamorphic zones must be defined. In fact, the two procedures yield similar results where the 10-Å peak is sharp and symmetric, (*i.e.,* for illitic I–S), but decomposition is difficult for a sharp asymmetric peak produced by a single illitic phase (Lanson, 1997).

This paper proposes a physical interpretation of the KI value by using a method that links KI, measured on both air-dried (AD) and ethylene-glycolated (EG) samples, to the mean number of the layers (N) in coherent scattering domains (CSD), and the percentage of smectite layers (%S) in I–S minerals. The proposed

†Deceased, 16 September 2000

method is also a rapid way to estimate N and %S. Eberl and Velde (1989) developed a similar method, based on KI and a measured peak intensity ratio IR, which was defined by IR = $(I_{001}/I_{003})_{AD}/(I_{001}/I_{003})_{EG}$ where $I_{00l(l=1,3)}$ is the measured intensity of a 00l peak, determined either on an AD or EG specimen (Środoń and Eberl, 1984). N and %S values are determined from a plot involving IR *versus* KI. This method, which requires five peak-parameter measurements (four related to intensities and one related to KI), can have significant error if quartz is present because the illite 003 and quartz 101 peaks overlap (Moore and Reynolds, 1997). Moreover, the background of the observed diffraction pattern is traced using a constant intensity value measured at the high-angle side of the 10-Å peak, which differs from the KI measurements. The alternative procedure which we propose in this paper requires only one measurement of the FWHM of the 10-Å peak on both air-dried (KIAD) and ethylene-glycolated (KIEG) samples, respectively. There is no peak-overlap problem with quartz. N and %S values are determined from various plots of KIAD *versus* KIEG which have been generated from data derived from many calculated XRD patterns using the NEWMOD computer program (Reynolds, 1985; Reynolds and Reynolds, 1996). A detailed procedure on generating the KIAD *versus* KIEG plots is presented to allow readers to construct similar charts. This method allows the KI limits of very low-grade metamorphism to be interpreted in terms of illite particle size (*i.e.,* N values).

PARAMETERS CONTROLLING 10-Å PEAK WIDTH

The 10-Å peak width of illite in an XRD pattern is a function of several interdependent parameters whose individual contributions are sometimes difficult to assess. Excluding instrumental peak broadening, illite crystal thickness is the main parameter that controls XRD peak width. According to Scherrer (1918), the FWHM of an XRD peak is inversely proportional to the size of the CSD generated by a single d value: $FWHM_{rad} = (\lambda \times K)/(T \times \cos \theta)$ where λ is the X-ray wavelength, K is the Scherrer constant, T is the thickness of the CSD, the subscript rad indicates radians and θ is the Bragg angle. This equation applies only if all CSDs have the same thickness, instrumental broadening is eliminated, and the structure factor and the Lorentz-polarization factor (Moore and Reynolds, 1997) do not vary significantly across the peak. By removing instrumental broadening only, Árkai *et al.* (1996) showed that the Scherrer equation yields an acceptable approximation of T, and therefore the mean number of illite layers N ($T = N \times d$; where d is the d value), in I–S with a low smectite content. If modified, the Scherrer equation can also be used directly for broad XRD peaks of I–S, without removal of instrumental effects, assuming that expandable interlayers are collapsed or the 002 illite peak of the AD pattern is used. Determination of the average of T ($\bar{T}$) is possible by estimating K for different CSD thickness distributions using XRD pattern simulations (Drits *et al.,* 1997) or experimental XRD data correlated with transmission electron microscope measurements (TEM) (Nieto and Sanchez-Navas, 1994). $\bar{T}$ determinations obtained using XRD techniques were corroborated by direct measurements of $\bar{T}$ using TEM observations (Eberl and Środoń, 1988; Merriman *et al.,* 1990; Eberl and Blum, 1993; Nieto and Sanchez-Navas, 1994; Árkai *et al.,* 1996; Dalla Torre *et al.,* 1996; Jiang *et al.,* 1997; Warr and Nieto, 1998). Mean thicknesses obtained from TEM and XRD analysis are comparable but both methods can be inaccurate if swelling layers are not considered.

Another fundamental parameter controlling the 10-Å peak broadening of illite minerals is the presence of expandable and sometimes chlorite-type layers (Reynolds, 1980). Hendricks and Teller (1942) demonstrated that interstratified I–S crystals with an infinite number of layers and variable d value produce a FWHM greater than zero (if no instrumental effect is considered), whereas it is zero for infinite crystals with a constant d value. Another source of FWHM broadening is disorder in the crystal structure (Reynolds, 1989), such as lattice strain which involves small variations in d value within CSDs of a single layer type (Drits and Tchoubar, 1990). Although lattice strain clearly affects KI values (Árkai *et al.,* 1996; Warr and Nieto, 1998; Drits *et al.,* 1998), its role is difficult to assess accurately in peak broadening analysis, because many authors interchange small variations of a single d value within one layer type with interstratification and CSD thickness (*e.g.,* Árkai *et al.,* 1996; Jiang *et al.,* 1997). According to Eberl *et al.* (1998a), the 10-Å peak is not significantly affected by strain. We believe that lattice strain is not sufficiently understood to be considered here.

Assumptions

The terms "illite" and "smectite" are used in the conventional sense; illite is a dioctahedral mica and smectite is a dioctahedral expandable phyllosilicate. We assume a unimodal distribution of the CSD thickness of I–S with a fixed variance for all mean N values, where %S is the mean smectite layer percentage. For a given %S, the distribution of the illite-smectite layer sequences in the CSD depends on the probability of finding an S layer as a first neighbor of an I layer or a second neighbor, *etc.* The number of consecutive layers whose type depends on the type of the first neighbor of the packet defines the Reichweite parameter, R (Jagodzinski, 1949). For instance, the distribution is binomial for R = 0 or random interlayering (Drits and Tchoubar, 1990). If R = 1, the probability

of an S layer next to an I layer is fixed. For the NEWMOD program, illite-rich I–S (R = 1) indicates that no S layers are consecutive. For the presented method, R follows the NEWMOD definition. Assuming N, %S, and R as the only factors controlling peak broadening, N and %S can be determined from two independent XRD measurements if R is fixed in value. Because the *d* value of expandable layers is dependent on the type of the interlamellar molecules (in this study, H_2O or ethylene glycol), KI determined from AD and EG specimens provides the required information.

If smectite is present, the interlayer is assumed to contain two molecule planes and thus KIAD measurements are larger than KIEG values. Two planes of H_2O molecules occur in Ca-exchanged samples with a relative humidity (RH) of ≥30% (MacEwan and Wilson, 1980; Eberl *et al.*, 1987), producing a smectite *d*(001) of ~15 Å. Broadening and asymmetry of the 5-Å peak is indicative of a single layer H_2O plane (Eberl *et al.*, 1987). These authors showed that RH also influences glycolated samples. For Ca-exchanged glycol-treated samples, a RH ≥10% results in *d*(001) of 17 Å, corresponding to two interlayer planes of EG. Specimens heated for ~12 h at 300°C and at a low RH are assumed to contain only 10-Å layers (Drits *et al.*, 1997).

KI limits and instrumental effect

Many diffractometers produce lower values (Kübler, 1990) than the original anchizone limits (0.42 and 0.25 °Δ2θ CuKα), as is the case for this study using a Rigaku diffractometer. Such values may be corrected using standards (Warr and Rice, 1994; Warr and Nieto, 1998). This was not necessary for this work because calibration was performed with the Philips diffractometer from Neuchâtel University, which was used to establish the original KI scale, hence the anchizone limits were set at 0.36 and 0.18°Δ2θ CuKα, respectively. These limits were calibrated using 27 samples measured on both diffractometers (Jaboyedoff, 1999).

To compare NEWMOD simulations to KI values, the instrumental peak broadening on experimental patterns must be removed. NEWMOD does not consider effects such as a flat specimen and axial divergence (Klug and Alexander, 1974; p. 290), and only the Lorentz-polarization factor is corrected (Reynolds, 1986). Instrumental broadening can be removed by deconvolution methods (Stokes, 1948; Ergun, 1968) or by the method described below, depending on the precision required.

METHODOLOGY

Sample preparation

The <2-μm clay size-fraction from HCl-dissolved limestone was extracted by centrifugation and Ca-exchanged with 1 M $CaCl_2$ twice every 24 h. Oriented clay aggregates were sedimented on a glass slide by using >3 mg/cm² of sample. The relative humidity for the AD specimen was >45%, the EG treatment was performed overnight in an EG atmosphere, and the specimen was heated at 450°C for 3 h. XRD data were recorded with a Rigaku horizontal powder diffractometer of 185 mm radius using a rotating Cu anode (CuKα radiation, nickel filter, 0.5° divergent and scatter slits, 0.15-mm receiving slit, and two 5° soller slits) at 40 kV and 30 mA.

Instrumental-broadening effect removal

For convenience, we use "illite width" (IW) for the 10-Å peak FWHM after removal of instrumental effects. Then IWAD corresponds to KIAD after removal of instrumental effects and IWEG to KIEG after removal of instrumental effects. A chart was constructed (Jaboyedoff, 1999) to obtain IW conveniently from KI measurements, assuming that the experimental 10-Å peak profile [h(2θ)] is the result of the convolution product [h(2θ) = f(2θ)*g(2θ)] of the instrumental profile [g(2θ)] and the pure clay mineral profile [f(2θ)] (Klug and Alexander, 1974; p. 291). The instrumental profile was determined experimentally using well-crystallized mica powders [g(2θ)], whereas the pure profiles were simulated with a Pearson VII function [f(2θ)] (with an exponential value of 2; Howard and Preston, 1989). KI are measured or calculated on the 10-Å peak profile, h(2θ), obtained by convolution, and IW on the pure clay mineral profile [f(2θ)]. Thus, a table of transformation is derived from measured KI to corrected IW. The XRD patterns were collected by continuous scans over the range 2–50°2θ CuKα at 2°/min with step sampling every 0.02°. Detailed XRD patterns were collected from 2 to 12°2θ CuKα by the step scanning method using 0.01° steps and a counting time of 2 s diagenesis-anchizone and anchizone-epizone limits, defined on the basis of KI measurements (0.25 and 0.42°Δ2θ CuKα, Philips diffractometer, Neuchâtel University), can be expressed in terms of IW values of 0.10 and 0.30°Δ2θ CuKα, respectively, with uncertainties of approximately ±0.02°Δ2θ CuKα (Jaboyedoff, 1999).

Extrapolation of NEWMOD-generated KI for > 100 layers

Isolines of %S and mean N on IWAD *versus* IWEG plots (Figures 1, 2, and 3) were constructed by measurement of IW on NEWMOD-generated patterns. The charts were constructed using swelling layers with two H_2O (2w) or two ethylene-glycol molecule (2g) layers, and are thus labeled IW2w and IW2g, respectively.

NEWMOD is limited to N = 100 layers. For N > 100, N and %S were derived from an empirical Scherrer equation, which assumed that IW increases proportionally with %S. Then, assuming a simple relationship between %S and N:

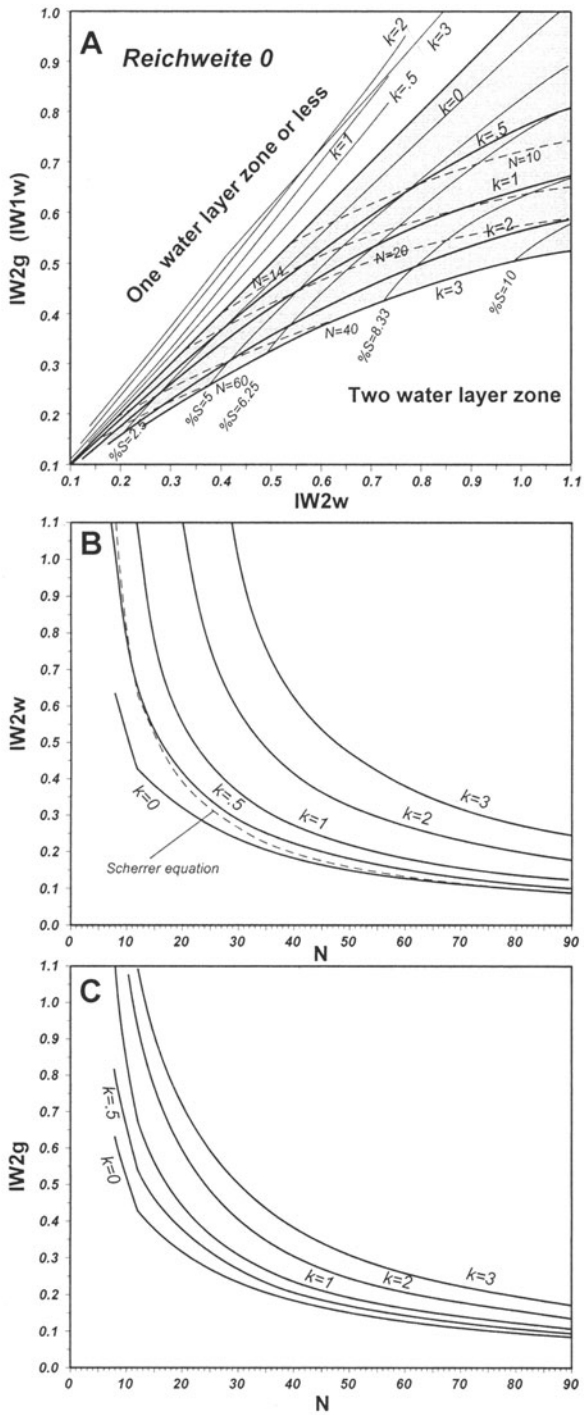

Figure 1. Charts used to determine N and %S based on the IW2w and IW2g of the 10-Å peak (°ΔCuKα IW) for Reichweite (R = 0) I-S. IWAD and IWEG are obtained by removing instrumental broadening from ICAD and ICEG. A) Chart used to estimate k based on IWAD and IWEG measurements. Note the upper position of the one-water layer *versus* two-ethylene-glycol (2g) k curves (Jaboyedoff *et al.*, 1999). B) Correspondence between N and IW2w for different k values. Curves for intermediate k values must be interpolated. Note the similarity with results using the Scherrer equation. C) Same as (B), but for IW2g. The shaded area in (A) indicates the zone where IW values have been evaluated.

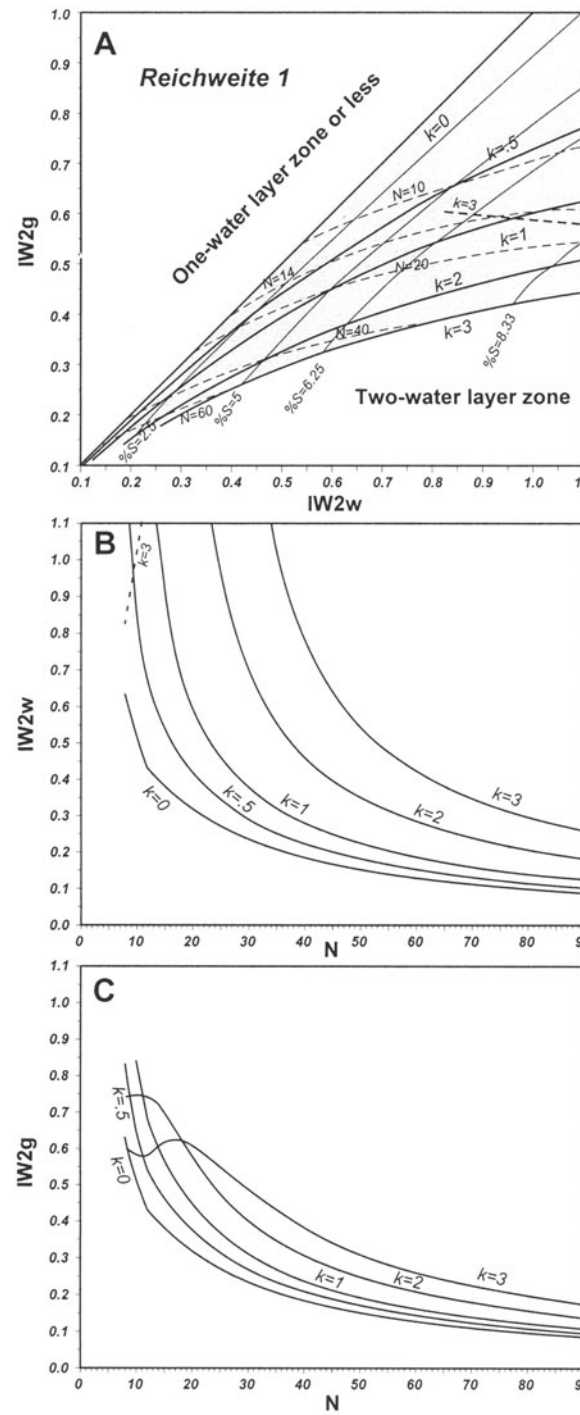

Figure 2. Same as Figure 1 but for (R = 1) I-S. The one-water layer k curves are not displayed. Note the decrease in IW2w (dashed line) for low N along the curve for k = 3 caused by the Reichweite value.

https://doi.org/10.1346/CCMN.2001.0490205 Published online by Cambridge University Press

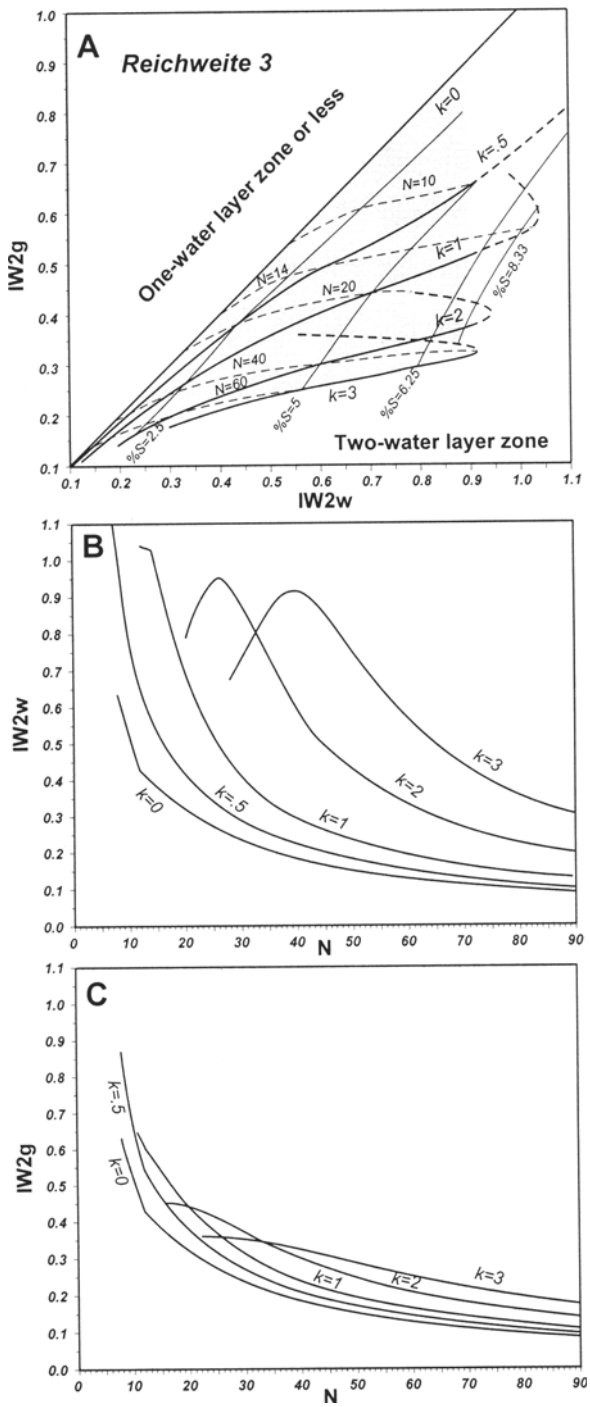

Figure 3. Same as Figure 2, but for (R = 3) I-S. The one-water layer k curves are not displayed. Note the decrease in IW2w for low N along curves for $k > 1$ caused by the Reichweite value. As for (R = 1) I-S, this decrease is associated with a significant migration of the diffraction peak. In this case, the validity zone is restricted to IW2w ≤ 0.9°ΔCuKα.

$$\frac{\%S}{100} = \frac{k}{N} \quad (1)$$

where k is a real number, it can be shown for N > 30 and a given k, that IW is related to N by (Jaboyedoff *et al.*, 1999):

$$IW = \frac{C_k}{N} \quad (2)$$

where C_k is an empirical constant determined by NEWMOD simulation, which is calculated for a given k and each treatment (AD and EG) by using simulations with large N (≥80). In an IW2w-IW2g graph, for high N values, the change in %S for a constant k value follows a straight-line relationship. Thus, k can be obtained from the plot of IWAD-IWEG. Equation (2) is used to determine N and %S using Equation (1) (Figure 1b). In a NEWMOD simulation, there are N − 1 interlayers. So, if N_s is the number of smectitic interlayers, $\%S = 100 \times (k/N) = 100 \times N_s/(N - 1)$ and then $k = N \times N_s/(N - 1)$. We have arbitrarily limited our model to $k = 3$, because most of the data are located in the field $k = 0$–3.

Chart construction

To find N and %S, for a given R, k is determined from IW2w *versus* IW2g charts, which display curves of constant k (k = 0, 0.5, 1, 2, 3). These curves are obtained by measurement of IW on NEWMOD simulated patterns for a fixed k value, which related N and %S by Equation (1). For N >90, Equation (2) is used because N is the mean of the thickness distribution ranging from N − 10 to N + 10. IW1w-IW2g charts were also calculated. Each chart involves >200 IW measurements from simulated patterns for each R value of 0, 1, and 3 (Figures 1, 2, and 3). Simulations were performed using the default parameters (d value of illite of 9.98 Å, smectite-2g of 16.9 Å, smectite-2w of 15 Å, smectite-1w of 12.5 Å; for Ca cation exchange). The following parameters were used: divergent slit 0.5°; goniometer radius 18.5 cm; sample length 2.8 cm, two soller slits of 5°; and chemistry $K_{0.9}(Al_{1.8},Fe_{0.2})(Si_{3.3},Al_{0.7})O_{10}(OH)_2$ for illite and $Ca_{0.165}(Al_{1.66},Fe_{0.2},Mg_{0.13})(Si_4)O_{10}(OH)_2$ for smectite. Because of the similarity between IW obtained from simulations with different distributions but identical mean and variance (Figure 4), we used a crystallite thickness density distribution with a constant value for the interval [N − 10; N + 10] and zero outside the interval. For N ≤ 12, the same constant thickness distribution density was used, but the non-zero value of the distribution belongs to the interval [2; (2N − 2)]. This choice was made to obtain a smooth peak, but causes an inflection in the curves at N = 12 on N *versus* IW charts because of the variance change of the number of layers in the CSDs.

https://doi.org/10.1346/CCMN.2001.0490205 Published online by Cambridge University Press

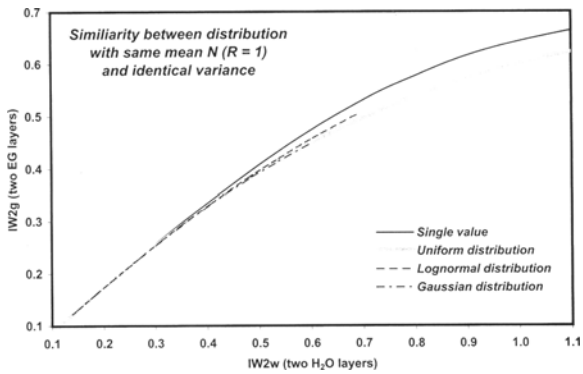

Figure 4. Comparison between k = 1 curves for (R = 1) I-S in an IW2w and IW2g chart showing good agreement between different distribution types of coherent diffracting domain sizes, where N and the variance are kept constant.

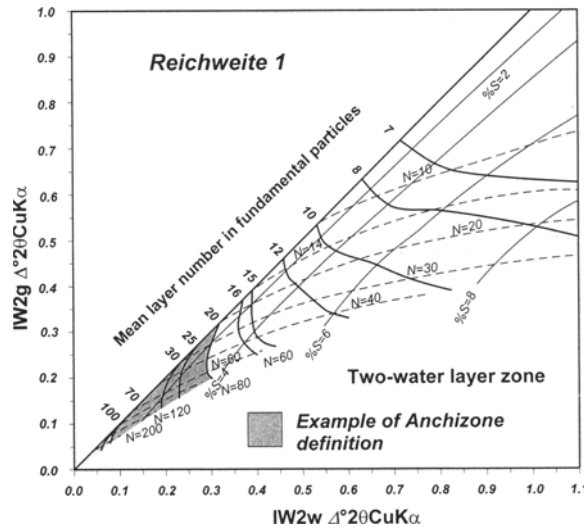

Figure 5. Graph of IW2w and IW2g for (R = 1) I-S with contours of N, %S, and N_{fp} values. Note that the fundamental-particle size contours are vertical in the vicinity of the anchizone.

By plotting the measured IWAD and IWEG values, k is estimated from the position of the curves of k values on the chart of IW2w *versus* IW2g (Figure 1a). N is obtained from Figure 1b or 1c, which displays various k curves, and their trajectories for changes in IW2w or IW2g. Finally, %S is computed with Equation (1). Figure 1b shows a family of curves sub-parallel to the curve obtained with the Scherrer equation; each corresponds to a different k value. Note that the line based on the Scherrer equation lies between the curve at k = 0 and k = 0.5.

The value of N determined from Figure 1b and 1c should be identical; if not, k must be reevaluated (Figure 1a) until there is acceptable agreement. This result may be compared to the result from the IW value from a heated specimen, assuming k = 0 (pure illite; *i.e.,* IW2w = IW2g). However, IW_{heated} must be determined with caution because its value depends on interlayer cation composition, heating temperature, and possible lattice strain induced by dehydration (Drits *et al.,* 1998).

RESULTS

Chart characteristics

With increasing value of k, curves migrate away from the axes and curvature increases (Figures 1, 2, and 3). For R = 0, R = 1, and R = 3, k-curves are similar, but become more widely spaced with increasing values for R. The direct use of charts for R > 0 is restricted to the shaded area in Figures 2a and 3a, where increases in IW2g are not matched by IW2w because of limiting %S and k values. This effect is observed for k = 2–3 for R = 1 (Figure 2b and 2c) and for k = 1–3 in the case of R = 3 (Figure 3b and 3c). These limiting conditions occur because peak migration caused by interstratification is sufficient to be observed. The peak-position method (Watanabe, 1988) may be used to evaluate %S, but N cannot be estimated by this method. As a consequence, the charts for R = 1 can be used for k values of 0–3 and IW2w of 0–1.1°Δ2θ CuKα, whereas for R = 3, the k-curves are more widely spaced and their usefulness is restricted to k = 0–3 and IW2w = 0–0.9°Δ2θ CuKα.

Curves of constant %S are subparallel to the diagonal of ratio 1:1 in all IW2w *versus* IW2g charts, with increasing curvature for the highest %S (Figures 1a, 2a, and 3a). Curves of constant mean N occur on the diagonal for pure illite IW with a gentle increase of IW2g toward the higher IW2w. In all IW2w *versus* IW2g charts, curves of constant mean number of layers in fundamental particles (constant N_{fp}) are correlated for low values and inversely correlated at high values. For KI values corresponding to anchizone, N_{fp} values have nearly constant IW2w values (*i.e.,* vertical N_{fp} isolines in Figure 5). For low RH values (15%), an IW1w *versus* IW2g chart is used because the points plot over the diagonal (IW1w < IW2g) (Figure 1a).

Example

A sample of anchizonal grade is discussed below to illustrate the accuracy of the method. The sample comes from a marly limestone of the Couches Rouges (Cretaceous) of the Prealps in Dimtigtal, Switzerland (Jaboyedoff and Thélin, 1996).

KI values of 0.34, 0.30, and 0.28°Δ2θ CuKα were determined for the AD, EG, and heated samples given respectively (Figure 6). Instrumental effects were removed by the method above, resulting in values of 0.29, 0.24, and 0.22°Δ2θ CuKα. The results shown in Figure 6 were obtained using Figures 1, 2, and 3, and N and %S were obtained for each Reichweite value (Table 1). The results are similar for all Reichweite values used. N varies by only five layers and %S

https://doi.org/10.1346/CCMN.2001.0490205 Published online by Cambridge University Press

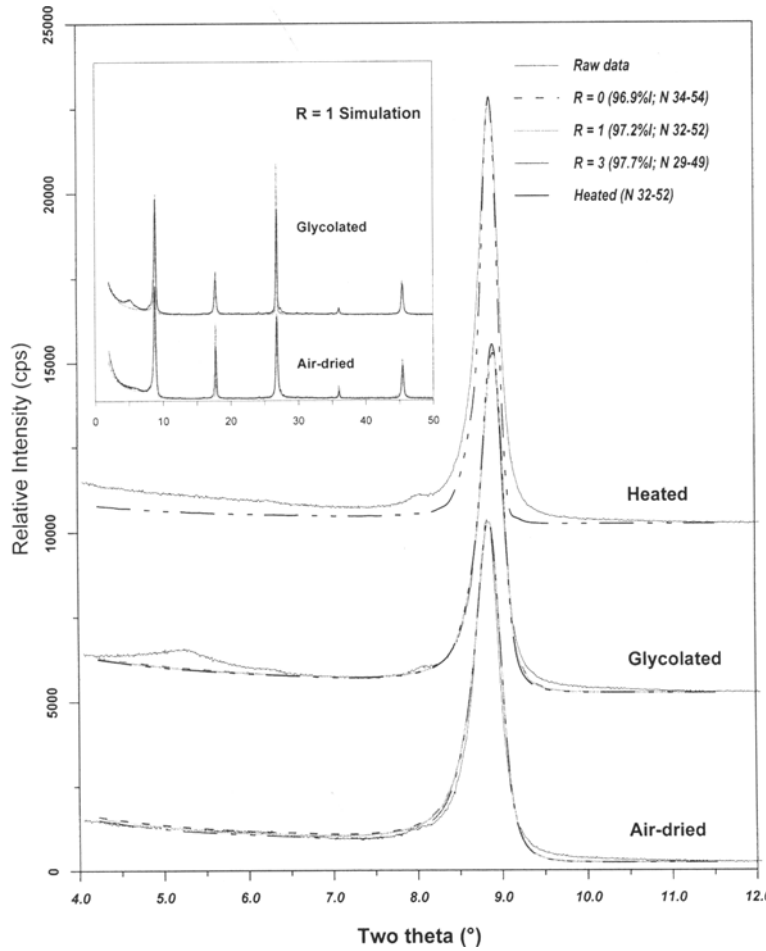

Figure 6. Comparison of a natural anchizonal XRD pattern with NEWMOD simulations based directly on this model (see Table 1). The sample is an oriented aggregate of the < 2-μm size fraction from a marly limestone in the Swiss Alps. To show the good agreement with peak shape, the positions of the 001 peaks are shifted (see text); computed diffraction intensities are multiplied by a variable coefficient (see text) and the added background is: intensity = 250 − 3 × °2θ value (cps).

varies from 2.3 to 3.1%. To compare NEWMOD simulations directly with raw data, the calculated diffraction patterns were convoluted with the profile of instrumental effects. The use of CuKα radiation instead of $CuK\alpha_1$ and $CuK\alpha_2$ introduces errors only when the IW is very small. On Figure 6, the 001 peak in the 2–12°2θ CuKα pattern is shifted by 0.06° for the EG and 0.05° for the AD pattern. The shifts occur because of the convolution effect; the central point of the powder XRD profile used for instrumental broadening is difficult to define. The 2–50° pattern was not convoluted, because the source profile differs over this range. For the small scan-range simulations, computed intensities were multiplied by: 1.70 for EG, 1.95 for AD, and 1.40 for the heated specimens. For large scan-range simulations, the factors were 1.53 for AD and 1.37 for EG specimens. These factors were used because glycolation causes misorientation and therefore peak intensities vary, whereas heating modifies grain geometry. The same linear background was applied to each pattern (y = 250 − 3 × °2θ). Simulations are in very good agreement with the experimental data. Note that IW values are sensitive to a few tenths of %S. In this respect, the NEWMOD version of 1985 is more appropriate than the version of 1996 where %S values are given to the nearest percent. Intensities of the higher order peaks do not fit (Figure 6), but this is probably partially related to chemical differences. The use of a $d(001)$ = 9.98 Å and the convolution process explains

Table 1. *k*, N, and %S values obtained with the proposed model for patterns of Figure 6.

Reichweite	*k*	N	%S
R = 0	1.36	34–54	3.1
R = 1	1.17	32–52	2.8
R = 3	0.91	29–49	2.3
Pure	0	22–42	0

https://doi.org/10.1346/CCMN.2001.0490205 Published online by Cambridge University Press

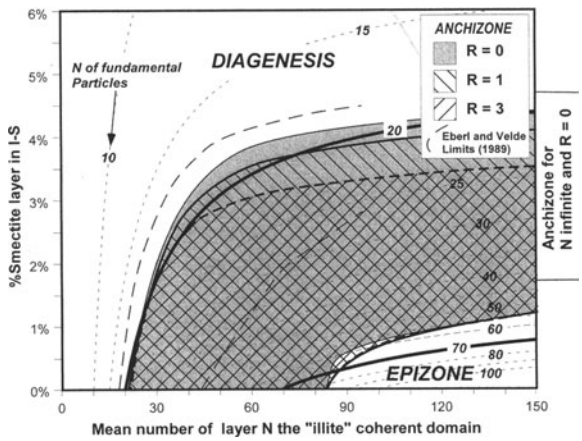

Figure 7. Plot of N *versus* %S of the two anchizone limits showing their similarity with constant fundamental-particle size curves in MacEwan particles.

the shift in peak positions. The intensities and peak-position variations in the higher order peaks of sedimented preparations may also be related to fine-particle segregation in the sedimented slide. Particle settling during sample preparation may favor coarser, more illitic minerals at the bottom of the oriented aggregate, leading to differences in intensities and peak positions of the higher order peaks.

The heated sample yields ~25% underestimation of N compared to the result obtained with the other treatments (mean N = 42). The simulated patterns for AD and EG are in better agreement with experimental data (Figure 6). The peak shape in the heated sample is slightly different from that in the computed pattern, indicating a disorder induced by dehydration (Drits *et al.,* 1998), different CSD thickness distributions, or the presence of unknown interstratification. In our experience, discrepancies between simulations and patterns of the heated specimen are common, whereas discrepancies are rare for other treatments. These results differ slightly from Eberl and Velde (1989) which yield IR = 1.3; N = 42, %S = 1.4% for uncorrected instrumental broadening effect and N = 60, %S = 1.2% after corrections.

SIGNIFICANCE OF THE KI ANCHIZONE LIMITS

Our method better defines the KI limits of very low-grade metamorphism in terms of N, %S, and R. The anchizone limits of the pure profile IW are estimated at KI (= KIAD) values of 0.10 and 0.30°Δ2θ CuKα. The N and %S paths of the limits are determined by fixing IW2w to the pure profile values and varying IW2g values over the entire range of valid values for the model (Figures 1a, 2a, and 3a). This procedure was applied to anchizone limits and to Reichweite values of R = 0, R = 1, and R = 3. On a plot of N *versus* %S, these limits display asymptotic behavior (Figure 7) towards infinite N. Here, large N values were computed for R = 0 as described in Hendricks and Teller (1942), and includes the Lorentz-polarization factor and the structure factor of illite. Figure 7 shows that the anchizone-epizone boundary has approximately the same N_{fp} value for R = 0, R = 1, and R = 3, but the anchizone-diagenesis limit has more significant variations especially for N > 30.

The relationship between N *versus* %S for MacEwan crystallites composed of fundamental particles of mean thickness (N_{fp}) is given by:

$$N_{fp} = \frac{N}{\left\{1 + \left[\left(\frac{\%S}{100}\right) \times (N - 1)\right]\right\}} \quad (3)$$

which is another form of the equation given by Środoń *et al.* (1990, 1992). The anchizone limits and N_{fp} curves follow a similar trend, as is shown in Figure 5. In a range of N = 0–100, and depending on the Reichweite, N_{fp} varies from 18 to 25 (IW2w = 0.30°Δ2θ CuKα) for the diagenesis-anchizone limit, and from 55 to 85 (IW2w = 0.10 °Δ2θ CuKα) for the anchizone-epizone limit.

DISCUSSION

The correspondence between N_{fp} and IW2w, and consequently between N_{fp} and KIAD for the anchizone limits (Figure 7) is the basis for the success of the KI method. The anchizone limits can be related to the range of fundamental particle mean thicknesses, given the precision and errors in KI measurements (Robinson *et al.,* 1990). The method described here indicates that this range is $20 < N_{fp} < 70$ for the anchizone (Figures 5 and 7), although these values are considered tentative. The significance of the KI scale is unambiguous in the limited range of anchizone and deep diagenesis, because it is the only range where constant N_{fp} for different N yields quasi-constant KI measurements (Figure 5). KI varies away from this range. Our results are in broad agreement with the anchizonal limits deduced from Eberl and Velde (1989), although they measure KI differently, which leads to higher estimate of N values (Figure 7). However, the correlation between the thickness of fundamental particles and degree of metamorphism does not favor any mechanism for the conversion of smectite to illite (Altaner and Ylagan, 1997).

For a fixed R, our model requires two parameters to allow a rapid estimation of %S, N_{fp}, and N. These values can be refined using NEWMOD simulations by varying size distributions or defect broadening, or by adding: (1) populations of I–S with different %S values and (2) different distributions of CSD thickness (*e.g.,* Pevear and Schuette, 1993; Jaboyedoff and Thélin, 1996). Three or more components within interstratified minerals (NEWMOD3c; Reynolds, 1988) may be

https://doi.org/10.1346/CCMN.2001.0490205 Published online by Cambridge University Press

Table 2. N values obtained by various authors for the anchizone limits. XRD arithmetic mean values of Dalla Torre *et al.* (1996) have been recalculated and high-resolution (HR)TEM values in parentheses are the values for the mode of the distribution.

Study	Diagenetic zone-anchizone (N)	Anchi-Epizone (N)	Method used
Particle thickness (without considering swelling layers)			
Weber *et al.* (1976)	15	28	XRD (Scherrer)
Merriman *et al.* (1990)	22	47	XRD (Scherrer) HRTEM (non applicable)
Krumm (1992)	22	50	XRD (Scherrer)
Nieto and Sanchez-Navas (1994)	30	90	HRTEM-XRD (Scherrer)
Warr and Rice (1994)	23	52	Warren-Averbach
Árkai *et al.* (1996)	~30	~60	W-A, Voigt, Scherrer, HRTEM
Dalla Torre *et al.* (1996)	28 (21)	65 (44)	XRD (Scherrer) - HRTEM
Jiang *et al.* (1997)	23	48	Scherrer
Merriman and Peacor (1999)	22	52	TEM
Fundamental particles thickness in MacEwan crystallites			
This study	~20	~70	NEWMOD and convolutions

modeled, but this was not explored here. The refinement of the results using NEWMOD may be necessary because the charts presented here are established for a given variance of the distribution of N. As shown in Figure 4, the distribution of N has a small effect on the peak shape for constant variance, but differences may occur for other variance values. Our model does not provide information about the possible mixture of I–S and illite populations, for instance, detrital micas mixed with neoformed I–S. In the sample of the above example, the detrital component was assumed to be <15%.

Limited data indicate that CSD thickness estimations based on TEM measurements may be greater than those based on XRD data. This may be attributed to mechanical cleaving during XRD sample preparation (Peacor, 1992; Li *et al.*, 1998) or to the difference in CSD thickness distributions between the whole rock and the <2-μm size fraction (Warr and Nieto, 1998). Árkai *et al.* (1996) noted that better agreement exists between TEM and calculated thickness based on the Scherrer equation than with other methods. Applying the principle of equivalence between N_{fp} and IW2w (IWAD), Árkai *et al.* (1996) may have measured the number of consecutive mica-like layers separated by swelling layers. Thus, it is not surprising that our results are apparently in accordance with the values of Weber *et al.* (1976), Krumm (1992), Merriman *et al.* (1990), Warr and Rice (1994), Árkai *et al.* (1996), Dalla Torre *et al.* (1996), and Jiang *et al.* (1997), all of whom used the Scherrer equation (Table 2). Our results are in accordance with the mean N of previous studies, 24 ± 5 (1σ) and 55 ± 17, for the anchizone lower and upper limits, respectively. Although XRD results obtained by Merriman *et al.* (1990) are in better agreement with the present study, their TEM results differ for the mean N value. This discrepancy may be related to detrital mica, the analysis of a coarser size fraction suggested by TEM observations (Jiang *et al.*, 1997; Warr and Nieto, 1998), strain broadening on XRD data (Warr and Nieto, 1998), or presence of expandable layers, which affect the XRD pattern and which may be overlooked by TEM.

The Bertaut-Warren-Averbach method is not relevant for interstratified clay minerals without special treatment (Warren and Averbach, 1950; Drits *et al.*, 1998; Eberl *et al.*, 1998a), as shown by Lanson and Kübler (1994). Accurate results may be obtained by removing the effect of swelling interlayers either by large scale expansion (Eberl *et al.*, 1998a) or by heating (Drits *et al.*, 1998). The KI properties for anchizone values (Table 2) may explain the good results of the Bertaut-Warren-Averbach method without using special treatment.

The removal of instrumental broadening may be a source of error for the absolute anchizone N_{fp} values, because of the difficulties in defining the pure profile (Árkai *et al.*, 1996). This effect may be very important for low IW, but the excellent match of the background at low angles (Figure 6) suggests the validity of the model.

The model assumptions of NEWMOD do not consider strain broadening. However, some strain is likely because the high- and low-angle side of the 00*l* peaks are often less sharp than those in the simulated patterns. This is attributed to strain, a few layers of paragonite or pyrophyllite or a NH_4-mica-like phase (Figure 6) or thin coherent diffracting domains.

The effects of parameters other than %S and N on the KIAD value are insignificant. On a regional scale, good correlation between the KIAD method and other metamorphic indicators (Kübler, 1984; Frey, 1987; Merriman and Frey, 1999) reflects the limited number of parameters controlling KIAD. Broadening relating to unexpected layers or lattice strain is limited because, if not, the KI scale would probably be more

irregular and not as useful for natural systems. Nevertheless, authors, such as Árkai *et al.* (1996) and Eberl *et al.* (1997), found that a low percentage of lattice strain (1–2%) leads to broadening. Furthermore, Árkai *et al.* (1996) found that lattice strain depends on a pressure-temperature (P-T) metamorphic path. Comparing their results with ours, the order of magnitude obtained for the limits of the anchizone is similar and thus probably correct. The lack of correlation concerning a link between strain and the MacEwan crystal concept supports our approach, but quantification of the lattice strain in interstratified clays will lead to an increase of the thickness limits of fundamental particles. Interstratification of pyrophyllite-like or other layer types with *d* value close to 10 Å probably cannot be differentiated from lattice strain.

Although increases in the mean grain size of minerals in isochemical systems with increasing metamorphic grade is a widely recognized trend, the specific process of crystal growth depends on many parameters, including nucleation rate, time, temperature, and reaction mechanism (Spry, 1983; Cashman and Ferry, 1988). For I-S, N_{fp} represents the size of illite crystals in one dimension only, but nevertheless this is a useful parameter to explore reaction history. Illite growth has been recognized as a time-dependent process (kinetic control) by many authors (Eberl and Hower, 1976; Bethke and Altaner, 1986; Pytte and Reynolds, 1989; Velde and Vasseur, 1992). For example, information about the growth rate and the reaction mechanism can be deduced from the size distribution (Cashman and Ferry, 1988) but, as shown by Eberl *et al.* (1998b), the growth mechanism cannot be deduced by inspecting the thickness distribution. However, the change of size distribution with increasing metamorphism does provide insights into crystal-growth history. Other parameters that control illite crystal growth, such as the effects of pressure or stress, still await detailed study.

CONCLUSION

The value of KI is related to two parameters, N and %S, for a given stacking order. The value of KI is sensitive to low percentages of expandable layers. Determining KI by the presented method requires two measurements (IWAD and IWEG), instead of five for the method of Eberl and Velde (1989), and simple software was developed to replace manual-chart reading. If KIAD is the only available reported measurement, the proposed method allows an estimation of the possible N and %S values. The sensitivity of the KI scale is maximized in the anchizone because of the relationship between KI and N_{fp} in this domain of incipient metamorphism (Kübler, 1968).

The similarity between the anchizone limits and the mean number of consecutive illite-like layers in I–S leads to a better definition of those zones. We propose that anchizone limits are between 20–70 N_{fp}, but recognize that this is tentative. Effects relating to unexpected layers other than I or S and strain broadening must be clarified and used to refine our model. Furthermore, despite the analysis of the clay-fraction, the presence of detrital mica is a source of sharpening of the diffraction peaks. The influence of detrital mica needs to be reduced further from standard KI measurements. However, strain and broadening effects from other layer types could well counterbalance the effect of detrital mica.

ACKNOWLEDGMENTS

Financial support was provided by the Swiss National Science Foundation, projects n° 21-26433.89 and 20-31234.91 and by the Dourakine Institute. R.C. Reynolds is thanked for his help with the NEWMOD program. Encouragement from T. Adatte, J.L. Epard, A. Escher, M. Maignan, and M. Sartori was greatly appreciated. S. Altaner, S. Guggenheim, and R.J. Merriman are also thanked for their manuscript improvements and English corrections. We thank the four anonymous reviewers for their constructive comments and English improvements. C. Bauchau, A.C. Jaboyedoff, and D. Kirschner are kindly thanked for their corrections.

REFERENCES

Altaner, S.P. and Ylagan, R.F. (1997) Comparison of structural models of mixed-layer illite/smectite and reaction mechanisms of smectite illitization. *Clays and Clay Minerals,* **45,** 517–533.

Árkai, P., Merriman, R.J., Roberts, B., Peacor, D.R., and Toth, M. (1996) Crystallinity, crystallite size and lattice strain of illite-muscovite and chlorite: Comparison of XRD and TEM data for diagenetic to epizonal pelites. *European Journal of Mineralogy,* **8,** 1119–1137.

Bethke, C.M. and Altaner, S.P. (1986) Layer-by-layer mechanism of smectite illitization and application to a new rate law. *Clays and Clay Minerals,* **34,** 136–145.

Cashman, K.V. and Ferry, J.M. (1988) Crystal size distribution (CSD) in rocks and the kinetics and dynamics of crystallization. III Metamorphic crystallization. *Contributions to Mineralogy and Petrology,* **99,** 410–415.

Dalla Torre, M., Livi, K.J.T., Veblen, D.R., and Frey, M. (1996) White K-mica evolution from phengite to muscovite in shales and shale matrix melange, Diablo Range, California. *Contributions to Mineralogy and Petrology,* **123,** 390–405.

Drits, V.A. and Tchoubar, C. (1990) *X-ray Diffraction by Disordered Lamellar Structures.* Springer-Verlag, Berlin, 371 pp.

Drits, V.A., Eberl, D.D., and Środoń, J. (1997) XRD measurement of mean crystallite thickness of illite and illite/smectite: Reappraisal of the Kubler Index and the Scherrer Equation. *Clays and Clay Minerals,* **45,** 461–475.

Drits, V.A., Eberl, D.D., and Środoń, J. (1998) XRD measurement of mean thickness, thickness distribution and strain for illite-smectite crystallites by Bertaut-Warren-Averbach technique. *Clays and Clay Minerals,* **46,** 38–50.

Eberl, D.D. and Blum, A. (1993) Illite crystallite thickness by X-ray diffraction. In *Computer Applications to X-ray Powder Diffraction Analysis of Clay Minerals, Volume 5,* R.C. Reynolds and J.R. Walker, eds., Clay Minerals Society, Boulder, Colorado, 124–153.

Eberl, D. and Hower, J. (1976) Kinetics of illite formation. *Geological Society of America Bulletin,* **87,** 1326–1330.

Eberl, D.D. and Środoń, J. (1988) Ostwald ripening and interparticle-diffraction effects for illite crystals. *American Mineralogist,* **73,** 1335–1345.

Eberl, D.D. and Velde, B. (1989) Beyond the Kübler index. *Clay Minerals,* **24,** 571–577.

Eberl, D.D., Środoń, J., Lee, M., Nadeau, P.H., and Northrop, H.R. (1987) Sericite from Silverton caldera, Colorado: Correlation among structure, composition, origin, and particle thickness. *American Mineralogist,* **72,** 914–934.

Eberl, D.D., Drits, V.A., and Środoń, J. (1997) Measurement of illite crystallite thickness by XRD method of Bertaut-Warren-Averbach. In *Journées Scientifiques en l'honneur de V.A. Drits,* Groupe Français des Argiles, Paris, 27–28.

Eberl, D.D., Nüesh, R., Sucha, V., and Tsipursky, S. (1998a) XRD measurement of fundamental particle thickness by X-ray diffraction PVP-10 technique. *Clays and Clay Minerals,* **46,** 89–97.

Eberl, D.D., Drits, V.A., and Środoń, J. (1998b) Deducing growth mechanisms for minerals from the shapes of crystal size distributions. *American Journal of Science,* **298,** 499–533.

Ergun, S. (1968) Direct method for unfolding convolution products: Its application to X-ray scattering intensities. *Journal of Applied Crystallography,* **1,** 19–23.

Frey, M. (1987) *Low Temperature Metamorphism.* Chapman & Hall, London, 351 pp.

Hendricks, S.D. and Teller, E. (1942) X-ray interference in partially ordered layer lattices. *Journal Chemical Physics,* **10,** 147–167.

Howard, S.A. and Preston, K.D. (1989) Profile fitting of powder diffraction patterns. In *Modern Powder Diffraction, Volume 20,* D.L. Bish and J.E. Post, eds., Mineralogical Society of America, Washington, D.C. 217–275.

Jaboyedoff, M. (1999) Transformations des interstratifiés illite/smectite vers l'illite et la phengite: Un exemple dans la série carbonatée du domaine Briançonnais des Alpes suisses romandes. Ph.D. thesis, University Lausanne, Switzerland, 459 pp.

Jaboyedoff, M. and Thélin, P. (1996) New data on the low-grade metamorphism in the Briançonnais domain of the Prealps, western Switzerland. *European Journal of Mineralogy,* **8,** 577–592.

Jaboyedoff, M., Kübler, B., and Thélin, P. (1999) An empirical Scherrer equation for weakly swelling mixed-layer minerals, especially illite-smectite. *Clay Minerals,* **34,** 601–617.

Jagodzinski, H. (1949) Eindimensionale Fehlordnung in Kristallen und ihr Einfluss auf Röntgeninterferenzen. I. Berechnung des Fehlordnungsgrades aus des Röntgenintensitäten. *Acta Crystallographica,* **2,** 201–207.

Jiang, W.T., Peacor, D.R., Arkai, P., Toth, M., and Kim, J.W. (1997) TEM and XRD determination of crystallite size and lattice strain as a function of illite crystallinity in pelitic rocks. *Journal of Metamorphic Geology,* **15,** 267–281.

Klug, H.P. and Alexander, L.E. (1974) *X-ray Diffraction Procedures.* J. Wiley and Sons, New York. 996 pp.

Krumm, S. (1992) Illite als Indikator schwacher Metamorphose. Methodische Untersuchungen, regionale Anwendungen and Vergleiche mit anderen Parametern. *Erlanger Geologische Abhandlungen,* **120,** 1–75.

Kübler, B. (1964) Les argiles indicateurs de métamorphisme. *Revue Institut Français du Pétrole,* **XIX(10),** 1093–1113.

Kübler, B. (1967) La cristallinité de l'illite et les zones tout à fait supérieures du métamorphisme. In *Etages tectoniques, Colloque de Neuchâtel 1966,* Edition de la Baconnière, Neuchâtel, Switzerland. 105–121.

Kübler, B. (1968) Evaluation quantitative du métamorphisme par cristallinité de l'illite. *Bulletin Centre de Recherche Pau SNPA,* **2,** 385–397.

Kübler, B. (1984) Les indicateurs des transformations physiques et chimiques dans la diagenèse, température et calorimétrie. In *Thermométrie et Barométrie Géologiques,* M. Lagache, ed., Société Française de Minéralogie et Cristallographie, Paris, 489–596.

Kübler, B. (1990) "Cristallinité" de l'illite et mixed-layer: Brève révision. *Schweitzerische Mineralogische Petrographische Mitteilungen,* **70,** 89–93.

Lanson, B. (1990) Mise en évidence des mécanismes de transformation des interstratifiés illite/smectite au cours de la diagenèse. Ph.D. thesis, University Paris 6, Paris, 366 pp.

Lanson, B. (1997) Decomposition of X-ray diffraction patterns (profile fitting): A convenient way to study clay minerals. *Clays and Clay Minerals,* **45,** 132–146.

Lanson, B. and Kübler, B. (1994) Experimental determination of coherent scattering domain size distribution of natural mica-like phases with the Warren-Averbach technique. *Clays and Clay Minerals,* **42,** 489–494.

Lanson, B. and Velde, B. (1992) Decomposition of X-ray diffraction patterns: A convenient way to describe complex I/S diagenetic evolution. *Clays and Clay Minerals,* **40,** 629–643.

Li, G., Peacor, D.R., Buseck, P.R., and Arkai, P. (1998) Modification of illite-muscovite crystallite-size distributions by sample preparation for powder XRD analysis. *Canadian Mineralogist,* **36,** 1435–1451.

MacEwan, D.M.C. and Wilson, M.J. (1980) Interlayer and intercalation complexes of clay minerals. In *Crystal Structures of Clay Minerals and their X-ray Identification,* G.W. Brindley and G. Brown, eds., Mineralogical Society, London, 197–248.

Merriman, R.J. and Frey, M. (1999) Pattern of very low-grade metamorphism in metapelitic rocks. In *Low-Grade Metamorphism,* M. Frey and D. Robinson, eds., Blackwell Science, Oxford, UK, 61–107.

Merriman, R.J., Roberts, B., and Peacor, D.R. (1990) A transmission electron microscope study of white mica crystallite size distribution in mudstone to slate transitional sequence, North Wales, UK. *Contribution to Mineralogy and Petrology,* **106,** 27–40.

Moore, D.M., and Reynolds, R.C. (1997) *X-ray Diffraction and the Identification and Analysis of Clay Minerals.* Oxford University Press, Oxford, 378 pp.

Nieto, F. and Sanchez-Navas, A. (1994) A comparative XRD and TEM study of the physical meaning of the white mica "crystallinity" index. *European Journal of Mineralogy,* **6,** 611–621.

Peacor, D.R. (1992) Diagenesis and low-grade metamorphism of shales and slates. In *Minerals and Reactions at Atomic Scale: Transmission Electron Microscopy,* P.R. Buseck, ed., Mineralogical Society of America, Washington, D.C., 335–380.

Pevear, D.R. and Schuette, J.F. (1993) Inverting the NEWMOD(c) X-ray diffraction forward model for clay minerals using genetic algorithms. In *Computer Applications to X-ray Powder Diffraction Analysis of Clay Minerals, Volume 5,* R.C. Reynolds and J.R. Walker, eds., Clay Minerals Society, Boulder, Colorado, 20–41.

Pytte, A.M. and Reynolds, R.C. (1989) The thermal transformation of smectite to illite. In *Thermal History of Sedimentary Basins Methods and Case Histories,* N. Naeser and R.C. McCulioh, eds., Springer-Verlag, New York, 133–140.

Reynolds, R.C., Jr. (1980) Interstratified clay minerals. In *Crystal Structures of Clay Minerals and Their X-ray Identification,* G.W. Brindley and G. Brown, eds., Mineralogical Society, London, 249–303.

Reynolds, R.C., Jr. (1985) *NEWMOD a computer program for the calculation of one-dimensional X-ray diffraction*

patterns of mixed-layered clays. R.C. Reynolds, Jr., 8 Brook Dr., Hanover, New Hampshire.

Reynolds, R.C., Jr. (1986) The Lorentz-polarization factor and preferred orientation in oriented clay aggregates. *Clays and Clay Minerals,* **34,** 359–367.

Reynolds, R.C., Jr. (1988) *NEWMOD3c for the calculation of one-dimensional X-ray diffraction patterns of mixed-layered clays containing three components.* R.C. Reynolds, Jr., 8 Brook Dr., Hanover, New Hampshire.

Reynolds, R.C., Jr. (1989) Diffraction by small and disordered crystals. In *Modern Powder Diffraction,* D.L. Bish and J.E. Post, eds., Mineralogical Society of America, Washington, D.C., 145–182.

Reynolds, R.C., Jr. and Reynolds, R.C., III (1996) *NEWMOD for Windows a computer program for the calculation of one-dimensional diffraction patterns of mixed-layered clays.* R.C., Reynolds, Jr., 8 Brook Dr., Hanover, New Hampshire.

Robinson, D., Warr, L.N., and Bevins, R.E. (1990) The illite 'crystallinity' technique: A critical appraisal of its precision. *Journal of Metamorphic Geology,* **8,** 333–344.

Scherrer, P. (1918) Bestimmung der grosse und inneren Struktur von Kolloidteilchen mittels Röntgenstrahlen. *Nachrichten Gesellschaft Wissenschaft Göttingen,* **26,** 98–100.

Spry, A. (1983) *Metamorphic Textures.* Pergamon International Libray, Oxford, UK, 352 pp.

Środoń, J. and Eberl, D.D. (1984) Illite. In *Micas,* S.W. Bailey, ed., Mineralogical Society of America. 495–544.

Środoń, J., Andreoli, C., Elsass, F., and Robert, M. (1990) Direct high-resolution transmission electron microscopic measurement of expandability of mixed-layer illite/smectite in bentonite rock. *Clays and Clay Minerals,* **38,** 373–379.

Środoń, J., Elsass, F., McHardy, W.J., and Morgan, D.J. (1992) Chemistry of illite-smectite inferred from TEM measurements of fundamental particles. *Clay Minerals,* **27,** 137–158.

Stokes, A.R. (1948) A numerical Fourier-analysis method for correction of widths and shapes of lines on X-rays powder photographs. *Proceedings of the Physical Society,* London, **61,** 382–391.

Velde, B. and Vasseur, G. (1992) Estimation of the diagenetic smectite to illite transformation in time-temperature space. *American Mineralogist,* **77,** 9–10.

Wang, H., Stern, W.B., and Frey, M. (1995) Deconvolution of the X-ray "Illite" 10 Å complex: A case study of Helvetic sediments from eastern Switzerland. *Schweitzerische Mineralogische Petrographischee Mitteilungen,* **75,** 187–199.

Warr, L.N. and Rice, H.N. (1994) Interlaboratory standardization and calibration of clay mineral crystallinity and crystallite size data. *Journal of Metamorphic Geology,* **12,** 141–152.

Warr, L.N. and Nieto, F. (1998) Crystallite thickness and defect density of phyllosilicates in low temperature metamorphic pelites: A TEM and XRD study of clay-mineral crystallinity-index standards. *Canadian Mineralogist,* **36,** 1453–1474.

Warren, B.E. and Averbach, B.L. (1950) The effect of cold work distortion on X-ray patterns. *Journal of Applied Physics,* **21,** 595–599.

Watanabe, T. (1988) The structural model of illite/smectite interstratified minerals and the diagram for its identification. *Clay Sciences,* **7,** 97–114.

Weaver, E.W. (1960) Possible uses of clay minerals in search for oil. *Bulletin of the American Association of Petroleum Geologists,* **44,** 1505–1518.

Weber, F., Dunoyer de Segonsac, G., and Economou, C. (1976) Une nouvelle expression de la "cristallinité" de l'illite et des micas. Notion "d'épaisseur apparente" des cristallites. *Compte Rendus Sommaires Société Géologique de France,* **5,** 225–227.

E-mail of corresponding author: michel.jaboyedoff@imp.unil.ch

(Received 1 June 1998; accepted 4 October 2000; Ms. 98-062)